Study on the effect of track curve radius on friction-induced oscillation of a wheelset-track system

Xiaolu Cui[1,2], Guangxiong Chen[2*], Huajiang Ouyang[3]

[1]*School of Mechanotronics & Vehicle Engineering, Chongqing Jiaotong University, Chongqing 400074, China*

[2]*State Key Laboratory of Traction Power, Tribology Research Institute, Southwest Jiaotong University, Chengdu, Sichuan 610031, China*

[3]*School of Engineering, University of Liverpool, Brownlow Street, Liverpool L69 3GH, UK*

Abstract

The purpose of the present paper is to investigate the correlation between the friction-induced oscillation of a wheelset-track system and curve radius and to explain a general phenomenon of rail corrugation based on the viewpoint of friction-induced oscillation. The typical phenomenon of rail corrugation in metros is that corrugation generally arises when the curve radius is quite small, whereas it rarely occurs when the curve radius is larger or on a straight track. Different multi-body models of the vehicle-track system and finite element models of the multiple-wheelset-track system with different curve radii are established respectively. According to the creep force analyses and unstable vibration analyses, the correlation between the creep force and friction-induced oscillation can be identified. Then, the effect of the track curve radius on the friction-induced oscillation of the wheelset-track system can be summarized, which provides an explanation of the typical phenomenon of corrugation.

*Corresponding author: Guangxiong Chen

E-mail address: chen_guangx@163.com

Keywords

Friction-induced oscillation; Creep force; Curve radius; Rail corrugation

Introduction

With the rapid development of urban railway construction, numerous problems of track degradation have been found. Rail corrugation is one of the most important kinds of track degradation. The research work on rail corrugation can be traced back to the beginning of the last century. So far, researchers have made significant progress in the investigation of the mechanisms of rail corrugation. Many endeavors have been made to understand and control the rail corrugations. According to the literature reviews [1, 2], the formation mechanism of rail corrugation is generally described by using the feedback loop [1], which mainly includes the damage mechanism and wavelength fixing mechanism. The damage mechanism is a physical process involving removal of material from the rail head surface, which mainly represents as wear and plastic flow of rail [3-5]. The wavelength fixing mechanism primarily reflects the dynamic behavior of wheel-rail systems, in which the corrugation wavelength is equal to the forward vehicle speed divided by the vibration frequency caused by the dynamic excitation between the wheel and rail. Normally, the vibrations of the wheel-rail system are caused by various excitation factors and have different frequencies. To confirm that which one of vibrations is the main reason to cause rail corrugation, two main schools of thought associated with the main wavelength fixing mechanism excitation in railways were proposed, which includes the theory of rail surface irregularity and the theory of instability of the wheel-rail system. In the theory of rail surface irregularity, it is considered that the frequency of wheel-rail transient dynamic interaction due to an initial rail surface roughness is related to the wavelength of rail corrugation [3-8]. Another theory believes that the main cause of corrugation

excitation is the instability of the wheel-rail system in some particular situations, which is related to the stick-slip oscillation [9-13] or the friction-induced oscillation [14, 15]. In the case of stick-slip oscillation, the oscillation mainly results from the periodic vibration of the normal contact force between wheel and rail near the saturation [9-12] or the negative slope of the friction-creepage relationship after saturation [13]. In the viewpoint of friction-induced oscillation, it is proposed that the friction-induced oscillation of the wheelset-track system is apt to occur when the creep force between the wheel and rail approaches saturation [14, 15]. In other words, the friction force leads to an asymmetric stiffness matrix and damping matrix of the wheel-rail system and hence the potential instability may occur.

Different phenomena of rail corrugation are studied based on the above viewpoints. It is well known that curved tracks are high incidence areas of rail corrugation and the track curve radius has an obvious influence on rail corrugation [16-19]. Wen et al. [16] researched the effect of scratch on rail corrugation on a curved track with radius 300 m when a wheelset passed through steadily and repeatedly. Saulot et al. [17] performed several tribological investigations of rail corrugation on a sharp curved track with radius 400 m. Torstensson et al. [18] studied the development of rutting corrugation on a 120 m-radius curved track by means of field measurements, laboratory experiments and numerical simulations. Eadie et al. [19] described the field evaluations of the effect of friction modifier on short corrugation growth on sharp curves with different radii less than 300 m. Meehan et al. [20] investigated the effect of non-uniformity in speed distribution on corrugation growth in curves and developed an efficient corrugation growth prediction model. Although the corrugation phenomena with specific curve radius have been researched, a typical phenomenon of rail corrugation remains a mystery, in which rail corrugation generally arises when the curve radius is

quite small, whereas it rarely occurs when the curve radius is larger or on a straight track. In Chinese metros, one clue of this typical rail corrugation is that the occurrence probability of rail corrugation on the low rail of the tight curved track is close to 100 percent, but the occurrence probability of rail corrugation on the high rail of the identical tight curved track is less than about 10 percent. Another clue is that both rails on the curved track whose curve radius is larger than 650-800 m rarely suffer from rail corrugation. Therefore, the purpose of the present paper is to research the afore-mentioned typical phenomena of rail corrugation in metros from the perspective of the correlation between the friction-induced oscillation of a wheelset-track system and curved track radius. Although the friction-induced oscillation is a possibility of rail corrugation, the viewpoint of the friction-induced oscillation has been verified by the field measurement [21], numerical simulation [14, 22] and experimental simulation [23]. In the present paper, the creep force analyses on different curve radii are made to identify the saturation of the creep force between the wheel and rail using the dynamic analyses of the multi-body models of vehicle-track systems. Then, the unstable vibration analyses on different curve radii are performed to study the stability of the wheelset-track systems using the complex eigenvalue analyses of the finite element models of wheelset-track systems. Therefore, the correlation between the creep force and the friction-induced oscillation of the wheelset-track system with different radii can be known. Furthermore, the effect of track curve radius on the friction-induce oscillation of the wheelset-track system can be summarized, which can provide an explanation of the typical phenomenon of rail corrugation.

Simulation model and numerical method

Wheelset-track contact model

Normally, the contact conditions between wheelsets and rails are different when a vehicle passes through curved tracks with different curve radii, especially on the leading wheelset. In the contact condition of single point between the wheel and rail, with the increase of the track curve radius, the contact point between the outer wheel and high rail of the leading wheelset gradually shifts from the wheel flange to the wheel tread, and shifts from the profile of rail head to the top of rail head. Even on a curved track with the same curve radius, the contact conditions between the leading wheelset and trailing wheelset also have significant differences. Figure 1 shows the wheelset-track contact model on a curved track. As for the force distribution of the wheelset-track system, the left (outer) and right (inner) vertical suspension forces (F_{SVL} and F_{SVR}), the lateral suspension forces (F_{SLL} and F_{SLR}) caused by the vehicle load are applied on the axle ends of the wheelset. When the wheelset rolls on a curved track, the normal contact forces (N_L and N_R) and creep forces (F_L and F_R) between the outer and inner wheels and rails are generated. The contact angle between the outer wheel and high rail is δ_L and that between the inner wheel and low rail is δ_R. In the track support structure, the rail and sleeper are connected by fastener, which is simulated by the spring and damper elements. Its vertical stiffness and damping are K_{RV} and $C_{RV,}$ and its lateral stiffness and damping are K_{RL} and C_{RL}, respectively. Besides, the sleeper is supported by the ballast and subgrade. The combined stiffness and damping of the ballast and subgrade also can be simulated by the spring and damper elements. The combined vertical stiffness and damping are K_{SV} and C_{SV} and the combined lateral stiffness and damping are K_{SL} and C_{SL}, respectively.

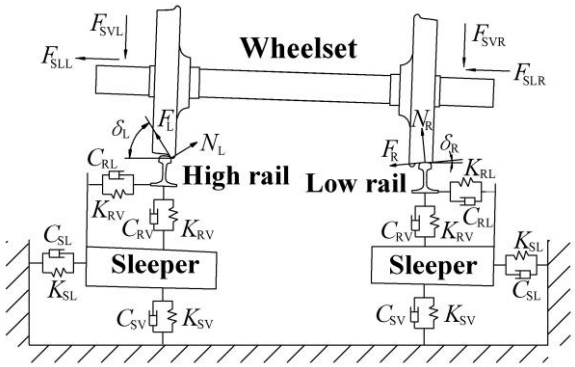

Figure 1. Wheelset-track contact model on a curved track

According to the wheelset-track contact parameters, to identify the specific contact conditions and force distributions between the wheelsets and rails, the multi-body models of the vehicle-track system on tracks with different curve radii are built and the dynamic analyses are carried out by Simpack. Then, the relevant finite element models of the multiple-wheelset-track system on tracks with different curve radii can be established using Abaqus.

Multi-body model of the vehicle-track system

The contact conditions and force distributions of the wheelset-track systems have evident differences due to the different curve radii. Hence the multi-body models of the vehicle-track systems with different curve radii built by Simpack are performed to calculate the corresponding parameters. The calculated lateral displacement and yaw angle of the wheelset can be used to define the specific contact points between wheels and rails in relevant finite element models. Additionally, the calculated vertical and lateral suspension forces of the wheelsets can be used to apply on the axle ends of each wheelset in the finite element models. Moreover, the obtained creep forces and normal contact forces between the wheels and rails can be used to judge whether the creep forces between wheels and rails are saturated or not.

The multi-body model of the vehicle-track system on a curved track supported by fixed-dual short sleepers established by Simpack is shown in Figure 2. The relevant parameters are listed in Table 1. The vehicle model is a simplified model of a regular passenger vehicle, which is made up of a carbody, two bogies with wheelsets connected by primary and secondary suspensions. The coefficient of friction is set as a constant, which is equal to 0.4. The track consists of a straight track of 50 m, a transition of 50 m and a curve of 200 m with a constant curve radius. The rail cants are all set as 1/40 and according to the actual conditions, the track gauges, track superelevations and average speeds of the vehicle with different curve radii are set as shown in Table 2 based on the "Maintenance Rule of Railway track" in China.

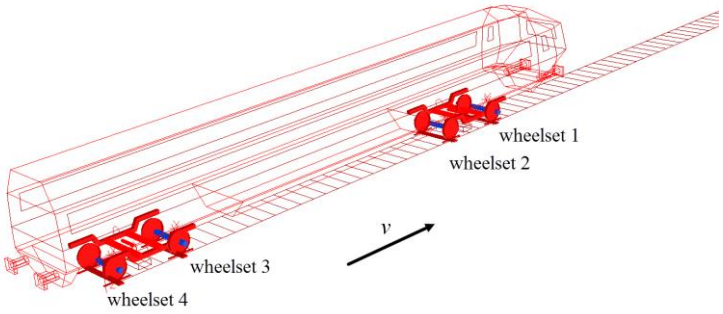

Figure 2. Multi-body model of the vehicle-track system

Table 1. Parameters of the multi-body model of the vehicle-track system

	Notation	Parameter	Value
Carbody	m_c (kg)	Mass of car body	23825
	I_{cx} (kgm^2)	Mass moment of inertia of car body	33832
	I_{cy} (kgm^2)	Mass moment of inertia of car body	528628
	I_{cz} (kgm^2)	Mass moment of inertia of car body	506504
Bogie	m_b (kg)	Mass of bogie	3970
	I_{bx} (kgm^2)	Mass moment of inertia of bogie around	2058
	I_{by} (kgm^2)	Mass moment of inertia of bogie around	2936
	I_{bz} (kgm^2)	Mass moment of inertia of bogie around	4716
Wheelset	m_w (kg)	Mass of wheelset	1654

		I_{wx} (kgm^2)	Mass moment of inertia of wheelset	726
		I_{wy} (kgm^2)	Mass moment of inertia of wheelset	100
		I_{wz} (kgm^2)	Mass moment of inertia of wheelset	726
Suspension	Primary	K_{px} (kN/m)	Stiffness of primary suspension alone	10000
		K_{py} (kN/m)	Stiffness of primary suspension alone	6500
		K_{pz} (kN/m)	Stiffness of primary suspension alone	1260
		C_{pz} (kNs/m)	Damping of primary suspension alone	10626
	Secondary	K_{sx} (kN/m)	Stiffness of secondary suspension alone	5000
		K_{sy} (kN/m)	Stiffness of secondary suspension alone	5000
		C_{sz} (kNs/m)	Damping of secondary suspension alone	2000
Track subsystem [4]		K_{RV} (MN/m)	Fastener vertical stiffness	40.73
		K_{RL} (MN/m)	Fastener lateral stiffness	8.79
		C_{RV} (Ns/m)	Fastener vertical damping	9898.70
		C_{RL} (Ns/m)	Fastener lateral damping	1927.96
		K_{SV} (MN/m)	Ballast vertical stiffness	89
		K_{SL} (MN/m)	Ballast lateral stiffness	50
		C_{SV} (Ns/m)	Ballast vertical damping	8.98×10^4
		C_{SL} (Ns/m)	Ballast lateral damping	4.0×10^4

Table 2. Track parameters with different curve radii

Curve radius (m)	200	250	300	350	400	450	500	550	600	650	700	750	800
Gauge (mm)	1450	1450	1440	1435	1435	1435	1435	1435	1435	1435	1435	1435	1435
Superelevation (mm)	120	120	120	120	120	100	100	90	70	70	60	60	50
Average Speed (km/h)	45	45	50	55	55	60	60	60	60	60	60	60	60

Finite element model of the wheelset-track system

Based on the wheelset-track contact model and the calculated parameters from the multi-body models of the vehicle-track systems, the corresponding finite element model of a multiple-wheelset-track system on a curved track supported by the fixed-dual short sleepers was established using Abaqus as shown in Figure 3. It is mainly composed of three parts, which includes four wheelsets, two rails and a series of sleepers. The relevant material parameters are listed in Table

3. As for the four wheelsets, the wheelsets 1 and 2 belong to the leading bogie, and the wheelsets 3 and 4 belong to the trailing bogie. The distance between two bogies is 7280 mm, and the distance between two wheelsets in the same bogie is 2200 mm. Therefore, the wheelsets 1 and 3 are leading wheelsets, and the wheelsets 2 and 4 are trailing wheelsets. The nominal diameter of the wheel is 840 mm and the wheel tread is LM-type tread normally used in Chinese metros. As for the curved tracks with different curve radii, the coefficients of friction are all set as 0.4 [14]. The standard track gauge is usually 1435 mm, but to keep the outer rail of curved track smooth and round, the track gauge is widened by traversing the inner rail. The track gauges are also set as shown in Table 2. The tracks are supported by fixed-dual short sleepers and the spacing between two sleepers is 625 mm. The DTVI2 fastener is used to connect the rail and sleeper, and the support stiffness and damping of the ballast is simulated by a series of spring-dashpot connections, as shown in Figure 3(b). The relevant parameters of the track support structure are the same as those in the multi-body model of the vehicle-track system, as shown in Table 1 [4].

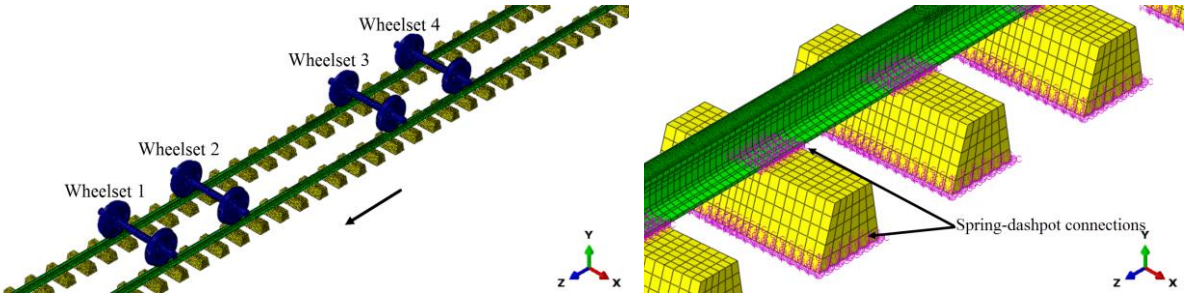

Figure 3. Finite element model of the multiple-wheelset-track system: (a) overview; (b) details of the spring-dashpot connections

Table 3. Material parameters of the multiple-wheelset-track system

Part	Density (kg/m^3)	Young's modulus (Pa)	Poisson's ratio
Wheelset	7800	2.1×10^{11}	0.3
Rail	7790	2.059×10^{11}	0.3
Sleeper	2800	1.9×10^{11}	0.3

Basic theory of corrugation wear

Wear is the process of gradual removal of material during the contact interaction in the relative motion. Hence rail corrugation phenomena are strictly associated with the frictional process between the wheel and rail. According to Archard's simplified wear theory shown in Equation (2-1), the relationship between the friction-induced oscillation of the wheel-rail system and corrugation wear also can be explained [24]. The model makes an assumption that the volume of removed material is proportional to the dissipated sliding energy duo to the friction force between two contact surfaces.

$$V = K\frac{N}{H}d \quad . \tag{2-1}$$

Taking the corrugated wear as an example, where V is the volume of removed material, N is the normal contact force between the wheel and rail, H is the hardness of rail, d is the relative sliding distance and K is the wear coefficient. K and H can be assumed as constants. Additionally, d also trends to be constant in a quasi-static state when the creep force trends to be saturated. Therefore, if the normal contact force varies with time due to the contact instability, the volume of removed material will vary as well in the process of wear. Similarly, according to the formula of rail abrasion presented by Brockley from the viewpoint of friction work between the wheel and rail [25], it also can be concluded that the variation of the friction work between the wheel and rail is largely influenced by the normal contact force between the wheel and rail.

Additionally, the variation of the normal contact force can be induced not only by the friction-induced oscillation, but also by the external-induced oscillation. To confirm which incentive is the main cause of rail corrugation, the dominant frequencies of friction-induced oscillation and external-induced oscillation are compared with the dominant frequency corresponding to the rail

corrugation. It can be found that the frequency of the friction-induced vibration of the wheelset-track system is consistent with the relevant oscillation frequency of rail corrugation in the field measurement, while other random vibrations may only bring about the stochastic wear of a point on the rail working surface, which cannot lead to rail corrugation [21]. The friction-induced oscillation of wheel-rail system generated by saturated creep force between the wheel and rail will lead to the oscillation of the normal contact force at the same frequency based on the mode coupling instability mechanism [26]. Moreover, the correlation between the friction-induced vibration and the fluctuation of the normal contact force has been studied by the comparison between the friction and frictionless condition using the transient dynamic analysis [22]. More details about the friction-induced oscillation and the resultant corrugation wear are studied in Ref. [27], in which the dynamic model of the wheel-rail system and wear model of rail corrugation are established. Therefore, it can be summarized that the friction-induced oscillation of wheelset-track system may induce rail corrugation.

Numerical method of the friction-induced oscillation

The mode coupling instability mechanism is one of the mechanisms of friction-induced instability, in which the friction force act as a follower force and destroy the symmetry of the stiffness and damping matrices resulting in flutter instability [26, 28]. The complex eigenvalue analysis is mainly adopted in the analysis of friction-induced instability of multi-DOF systems, which can accurately forecast the stability of the system in frequency domain [29]. The unstable oscillation frequency and corresponding mode of the friction-induced instability also can be obtained. The theoretical methodology of the complex eigenvalue analysis is briefly described as below [29].

Generally speaking, the motion equation of a discrete mechanical system in the quasi-static stability state can be written as:

$$[M]\ddot{x}+[C]\dot{x}+[K]x=q, \tag{2-2}$$

where [*M*], [*C*] and [*K*] stand for the symmetric mass, damping and stiffness matrix, respectively. *q* is the vector of the generalized external forces. *x* stands for the nodal displacement vector, which includes all the degrees of freedom.

In the numerical simulation of the friction-induced stability of the wheelset-track system, due to the effect of friction between the wheel and rail, the motion equation of the wheel-rail system can be rewritten in the following form:

$$[M_f]\ddot{x}+[C_f]\dot{x}+[K_f]x=0, \tag{2-3}$$

where [M_f], [C_f] and [K_f] stand for the asymmetric mass, damping and stiffness matrices due to friction, respectively. Since the global mass, damping and stiffness matrix are asymmetric, the system might manifest flutter instability of various modes of the system. In addition, the stronger the asymmetric is, the friction-induced oscillation more easily occurs.

The corresponding eigenvalue equation can be expressed as:

$$(\lambda^2[M_f]+\lambda[C_f]+[K_f])\phi=0, \tag{2-4}$$

where λ stands for the eigenvalue and ϕ stands for the corresponding eigenvector. Then, the general solution can be obtained using the subspace iteration method.

$$x(t)=\sum_{k=1}^{n}\phi_k e^{\lambda_k t}, \tag{2-5}$$

where ϕ_k is the *k*th eigenvector. λ_k is the *k*th eigenvalue, which can be expressed by means of its real and imaginary part, that is, $\lambda_k=\alpha_k+i\omega_k$. The real part of the eigenvalue, α_k, represents the stability of the system. The imaginary part of the eigenvalue, ω_k, represents the steady-state circular

frequency of the system. When the real part of an eigenvalue is larger than zero, the unstable vibration of the system primarily takes place, which means that the vibration amplitude grows exponentially with time even under a small perturbation.

Additionally, another parameter to judge the stability of the wheelset-track system in the complex eigenvalue analysis in Abaqus is the effective damping ratio, which is defined as:

$$\xi_k = \frac{-2\alpha_k}{|\omega_k|}. \tag{2-6}$$

Adams proposed that the effective damping ratio, rather than the real part of the eigenvalue, was taken as the measure of the severity of the instability for the same reason that it was used for positively damped systems [30]. Positive effective damping ratio ($\xi_k > 0$) corresponding to stable motion ($\alpha_k < 0$), whereas negative damping ratio ($\xi_k < 0$) represented unstable (self-excited) motion ($\alpha_k > 0$) [30]. Furthermore, the smaller the negative effective damping ratio is, the corresponding friction-induced oscillation more easily occurs.

In the finite element analysis of the friction-induced oscillation of the wheelset-track system, the effective damping ratio of the wheelset-track system can be directly extracted by the complex eigenvalue analysis using Abaqus. The procedures of numerical simulation are introduced as follows. Firstly, the vertical and lateral suspension forces are imposed on the axle ends of each wheelset. The corresponding parameters result from the calculations using Simpack. Then, the lateral and longitudinal relative slipping velocities are applied on the wheels using the quasi static analysis. After that, the natural frequencies of the wheelset-track system are extracted using the mode analysis. Finally, the unstable vibration frequency and the relevant mode can be obtained using the complex eigenvalue analysis. Moreover, it is hypothesized that the rail surface is utterly smooth. Only the suspension forces are applied on the wheelsets and no other disturbance exists. Therefore, the

predicted unstable oscillation of the wheelset-track system in numerical simulation is the friction-induced oscillation.

Results and discussion

Numerical results of vehicle curve negotiation

According to the Simpack simulation results, the specific contact points and the force distributions between the wheelsets and tracks can be identified. The contact points between different wheelsets and rails can be confirmed via selecting the average values of lateral displacement and yaw angle in the stability range of the vehicle. Figure 4 shows the distributions of lateral displacement and yaw angle of each wheelset on tracks with different curve radii. It can be found that the contact points of the wheelsets 1 and 3 of the leading wheelsets are quite similar. With increasing the curve radius, the absolute value of the lateral displacement of the leading wheelset decreases. The abrupt change from 200 m to 350 m is mainly due to the variation of track gauge. In addition, the absolute value of the yaw angle of the leading wheelset decreases obviously with increasing the curve radius. Therefore, the contact point between the outer wheel of the leading wheelset and high rail gradually shifts from the wheel flange to the wheel tread, and shifts from the profile of rail head to the top of rail head with increasing the track curve radius, which means the relevant contact angle decreases. The contact point between the inner wheel of the leading wheelset and the low rail is generally located between the wheel tread and the top of rail head with increasing the track curve radius, which means the relevant contact angle changes slightly. Besides, the contact conditions of the wheelsets 2 and 4 of the trailing wheelsets are quite similar. With increasing the curve radius, the absolute values of the lateral displacement and yaw angle change slightly except those values in the radius range of

200-350 m. The contact points of trailing wheelset are usually situated between the wheel tread and the top of the rail head with increasing the track curve radius, which means the contact angles changes slightly.

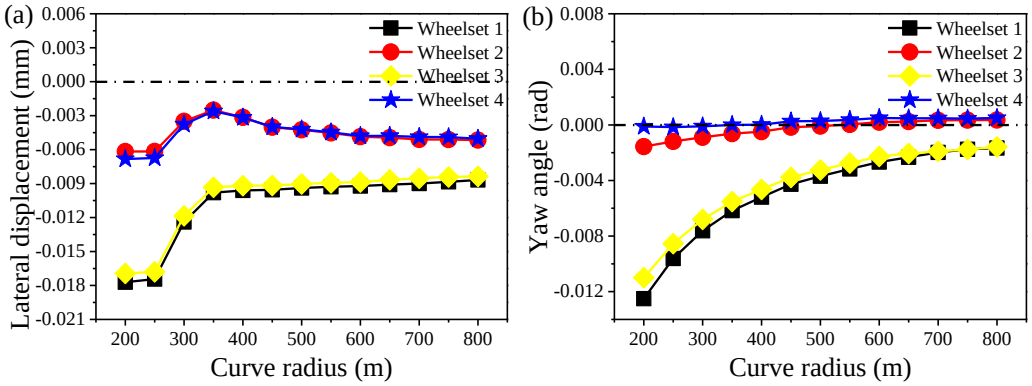

Figure 4. Distributions of lateral displacement and yaw angle of each wheelset on tracks with different curve radii: (a) lateral displacement; (b) yaw angle

In addition, the force evolution of the wheelset-track systems also can be calculated. Firstly, the vertical and lateral suspension forces imposed on the axle ends of the wheelsets are obtained, which are the average values of the suspension forces in the steady state of vehicle curve negotiation and the results are shown in Figures. 5-6. Figure 5 shows the evolution of the vertical suspension forces of left and right wheels of each wheelset. It can be found that the evolutionary tendencies of the vertical suspension forces on the left and right wheels of the same wheelset are symmetrical. Figure 6 shows the evolution of the lateral suspension forces of left and right wheels of each wheelset. It can be found that the evolutionary tendencies of the lateral suspension forces on the left and right wheels of the same wheelset are consistent. Because only the vertical and lateral suspension forces are applied on the axle ends of each wheelset in the finite element models and the tracks are completely smooth, the unstable oscillations of the wheelset-track system generated in the running process are friction-induced oscillations.

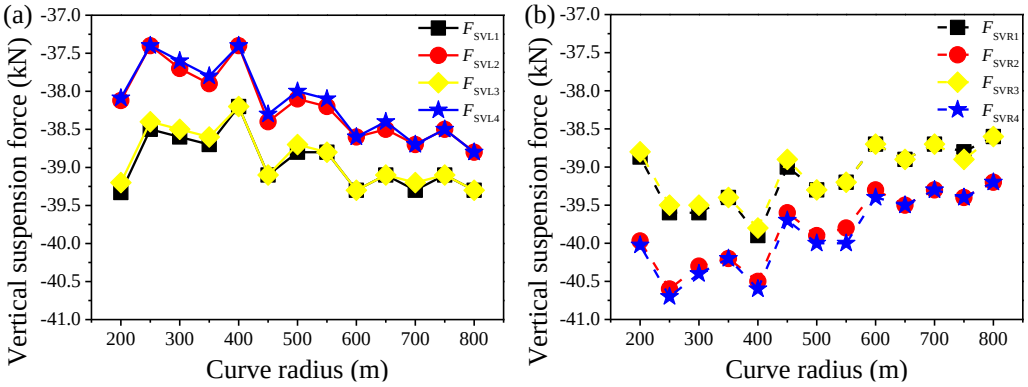

Figure 5. Evolution of the vertical suspension force of each wheelset on tracks with different curve radii: (a) left wheel; (b) right wheel

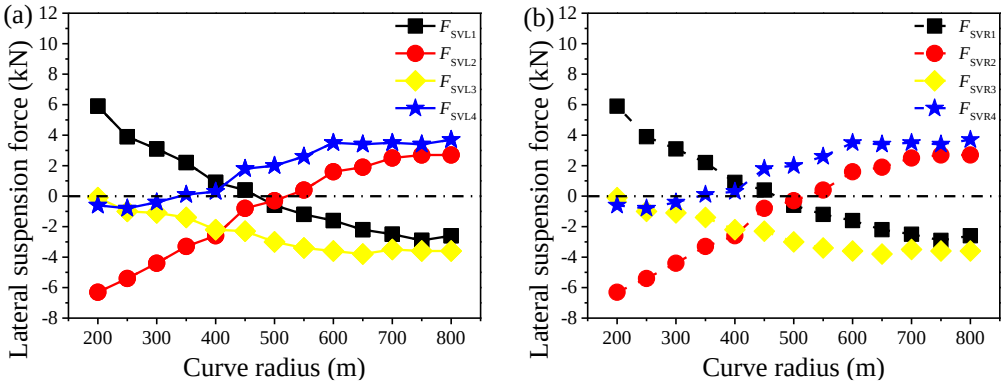

Figure 6. Evolution of the lateral suspension force of each wheelset on tracks with different curve radii: (a) left wheel; (b) right wheel

Creep force analyses in different curve radii

The value of the creep force is limited by the maximum friction force when it reaches saturation. Whether the creep force is saturated can be estimated by comparing the creep force resultant and friction force. The creep force resultant is equal to the resultant of the longitudinal and lateral creep forces. The friction force is equal to the normal contact force multiplied by the coefficient of friction and the coefficient of friction is set as 0.4. According to the Simpack simulation, the lateral, longitudinal and normal contact forces between the wheel and rail can be obtained. Then, the creep force resultant and friction force between the wheel and rail can be calculated. For instance, the

comparisons between the creep force resultants and friction forces between the wheels and rails are shown in Figure 7 at a curve radius of 200 m. It can be found that the creep forces on both wheels of the wheelsets 1 and 3 are clearly saturated. The creep forces on both wheels of the trailing wheelsets are unsaturated.

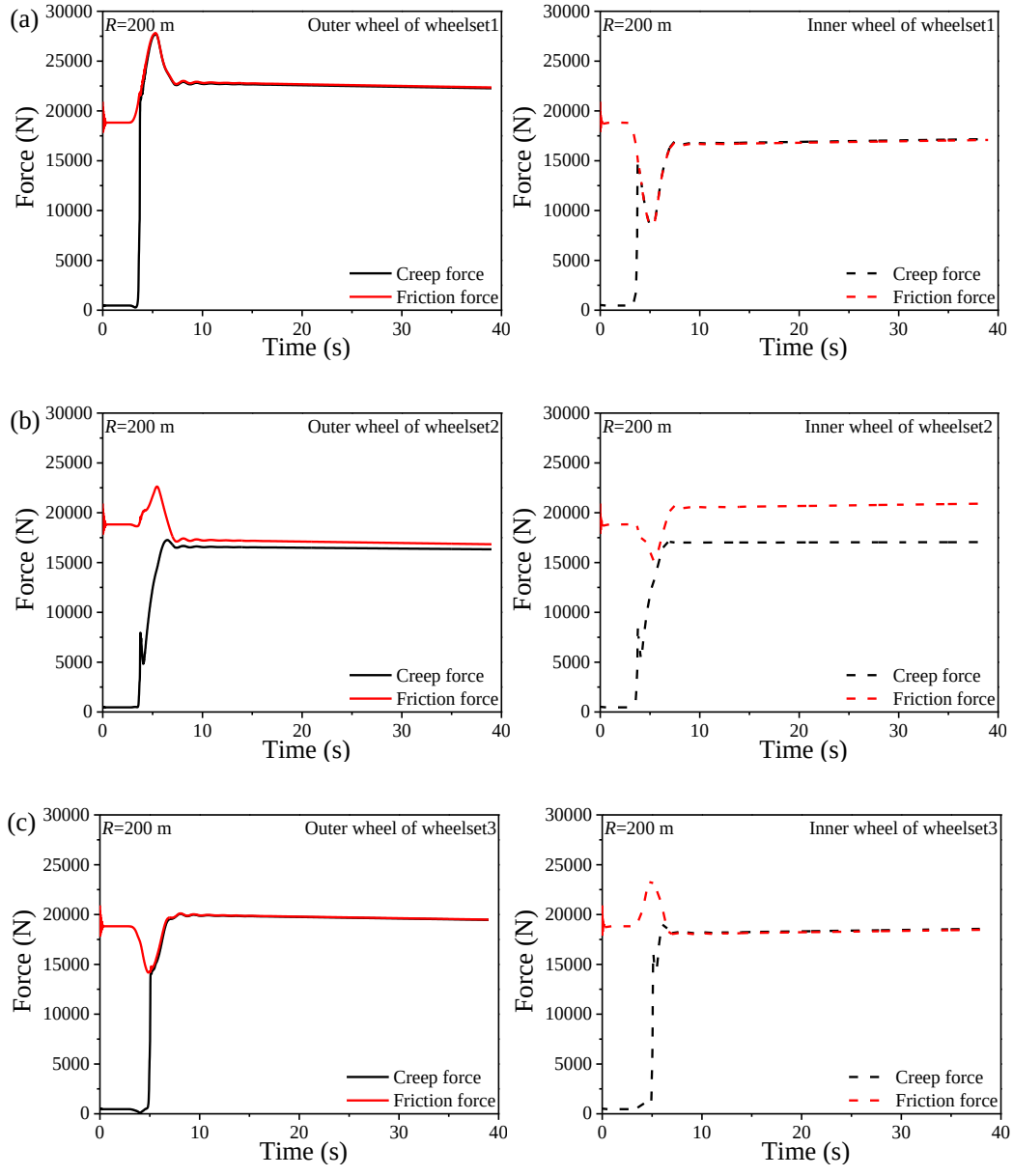

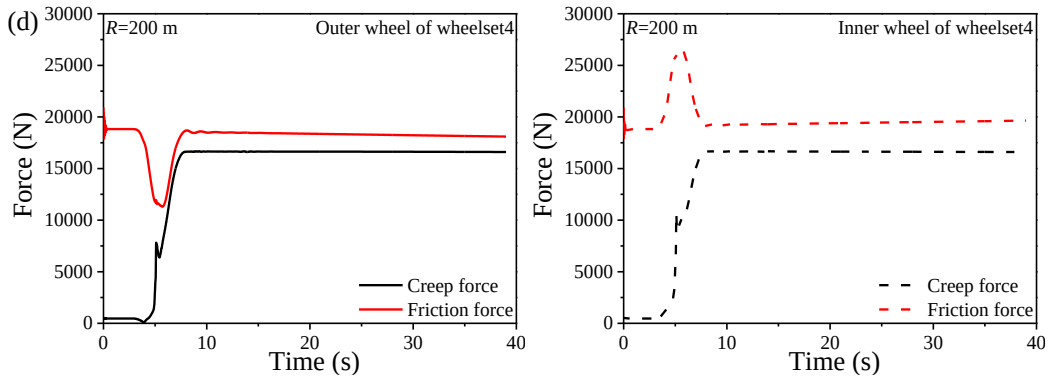

Figure 7. Comparisons between the creep force resultants and friction forces (R = 200 m): (a) Wheelset 1; (b) Wheelset 2; (c) Wheelset 3; (d) Wheelset 4

Correspondingly, the creep force resultants and friction forces on the tracks with curve radius from 200 m to 800 m also can be calculated. In order to state the comparisons between the creep force resultants and friction forces on the tracks with different curve radii more definitely, the deviation between the creep force resultant and friction force of each wheel in the static state can be adopted, which is defined as:

$$\varepsilon = \frac{(F_{f\max} - F_c)}{F_c}, \tag{3-1}$$

where ε is the deviation. $F_{f\max}$ is the friction force in the static state. F_c is the creep force resultant in the static state. The evolution of deviations in the static state is shown in Figure 8. It is assumed that the creep force between the wheel and rail can be regarded as saturated when the deviation is quite small. With the curve radius growing from 200 m to 800 m, the creep force on the outer wheel of the leading wheelset always approaches to be saturated, while that on the inner wheel of leading wheelset gradually trends to be unsaturated. The creep forces on both wheels of leading wheelset trend to be saturated when the curve radius is less than 450 m. However, the creep forces on both the outer and inner wheels of the trailing wheelset are obviously unsaturated in the curve radius range of 200-800 m.

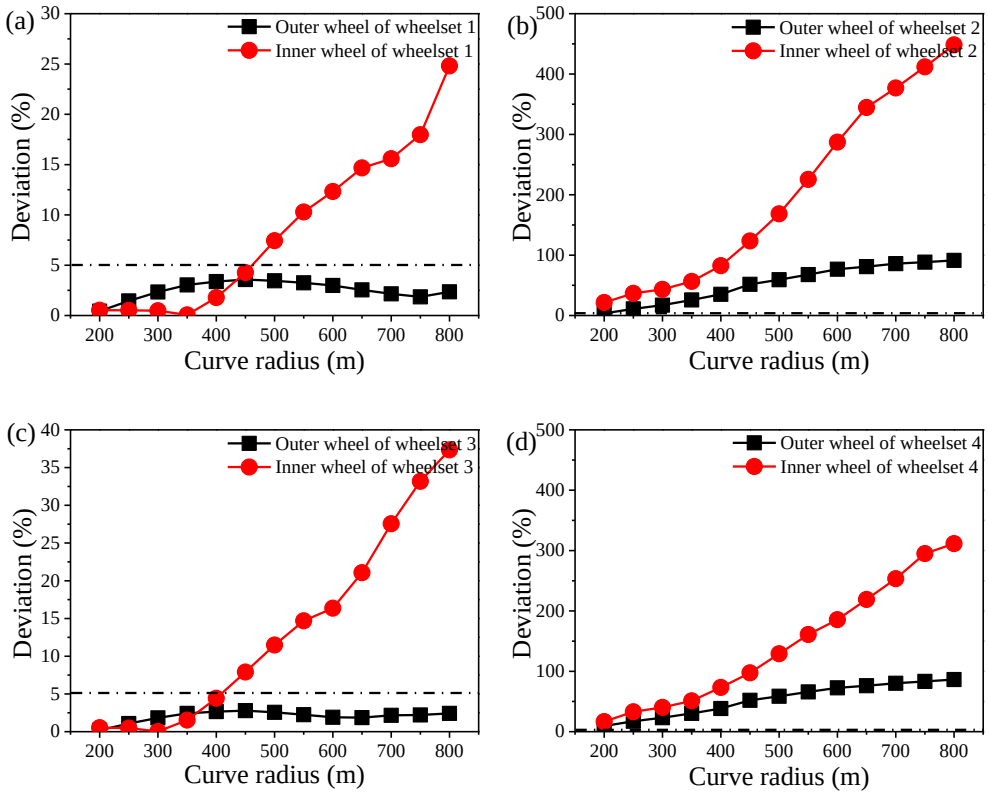

Figure 8. Variation of the deviations between the creep force and friction force with curve radius: (a) Wheelset 1; (b) Wheelset 2; (c) Wheelset 3; (d) Wheelset 4

Unstable vibration analyses in different curve radii

According to the numerical results of vehicle curve negotiation in Section 3.1, the specific contact points and the forces between the wheelsets and tracks can be identified. After judging whether the creep forces between wheels and rails are saturated in Section 3.2 and applying the corresponding relative slipping velocities on the wheels with different curve radii, the friction-induced oscillations of the wheelset-track systems can be further studied. Then, the unstable vibration analyses in different curve radii are studied using the complex eigenvalue analysis.

The effective damping ratio calculated by the complex eigenvalue analysis is an important parameter to evaluate the stability of the wheelset-track system. The unstable oscillation of the wheelset-track system may occur in the case of negative effective damping ratio. Additionally, the

smaller the effective damping ratio is, the corresponding friction-induced oscillation more easily occurs. Figure 9 shows the distributions of the negative effective damping ratios of wheelset-track systems with different curve radii. Because the friction-induced oscillation corresponding to the smallest negative effective damping ratio is most likely to occur, it is necessary to pay attention to the evolution of the smallest negative effective damping ratio with different curve radius. It can be found that the value of the smallest effective damping ratio gradually increases when the curve radius changes from 200 m to 500 m. When the curve radius changes from 550 m to 800 m, no negative effective damping ratio exists. In summary, the friction-induced oscillation of the wheelset-track system is apt to occur when the curve radius is less than 500 m, and the occurrence possibility decreases gradually from radius 200 m to 500 m. Then, when the curve radius is larger than 500 m, the friction-induced oscillation rarely occurs.

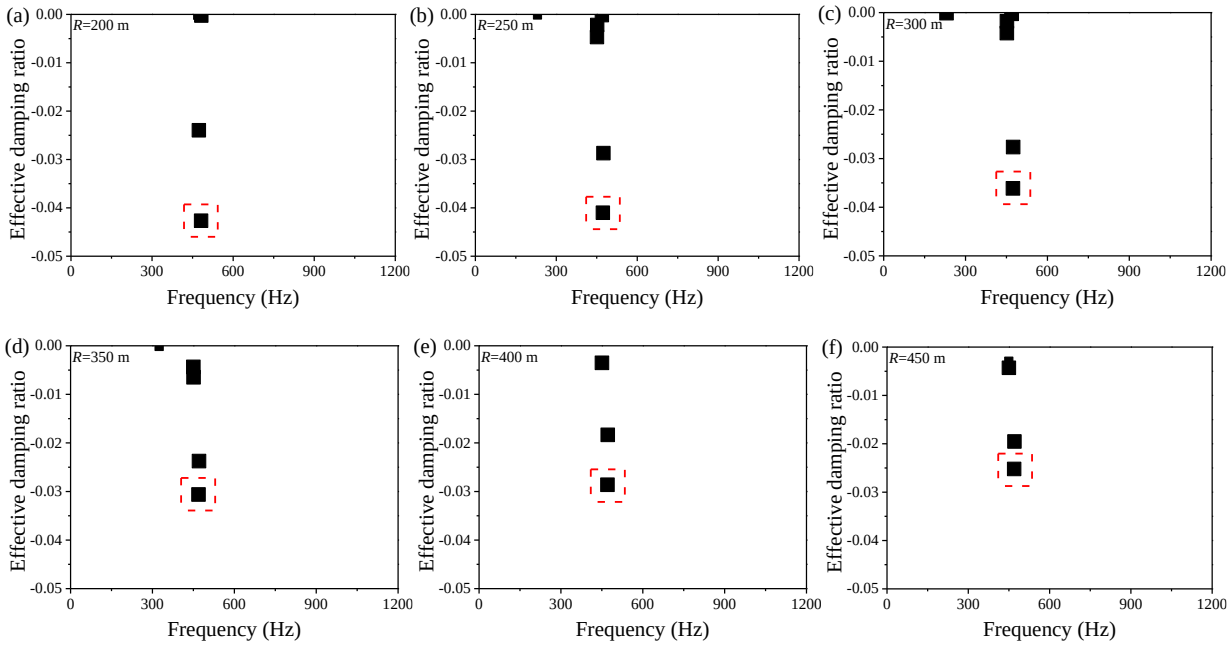

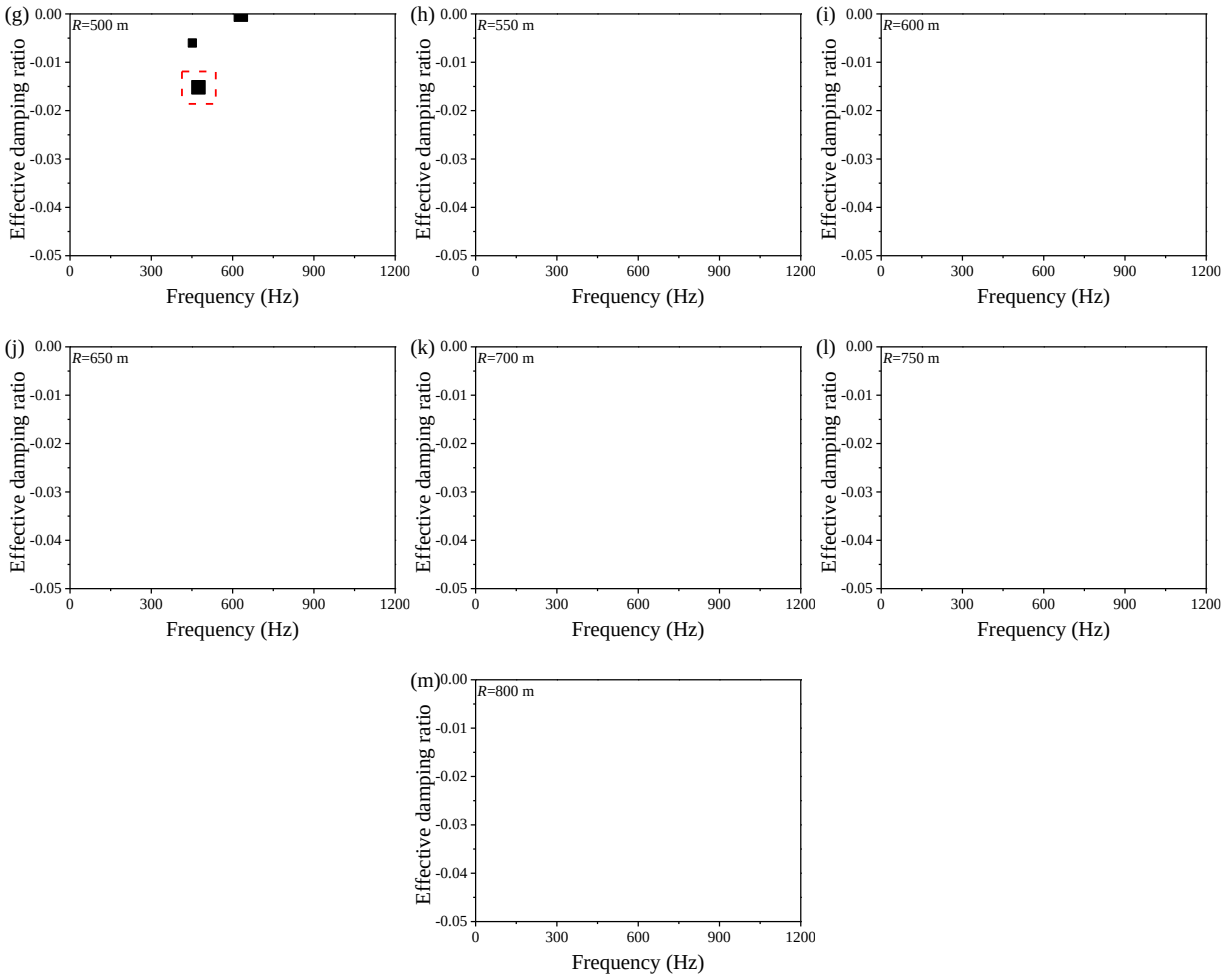

Figure 9. Distributions of the negative effective damping ratios of the wheelset-track systems for different curve radii: (a) R = 200 m; (b) R = 250 m; (c) R = 300 m; (d) R = 350 m; (e) R = 400 m; (f) R = 450 m; (g) R = 500 m; (h) R = 550 m; (i) R = 600 m; (j) R = 650 m; (k) R = 700 m; (l) R = 750 m; (m) R = 800 m

From Figure 9, it also can be found that the number of the negative damping radius is largest at the curve radius of 300 m, which corresponds to most of the potentially unstable vibration modes of the wheelset-track system on curved tracks. The relevant frequencies and mode shapes of unstable vibrations with radius 300 m are shown in Figure 10. From the mode shapes of Figure 10(a) and (b), the unstable oscillations of the wheelset-track system probably take place on both rails and two wheels. But the unstable oscillations hardly occur because the negative effective damping ratios are fairly close to zero [14]. Then, from the mode shapes of Figure 10(c) to (h), the unstable oscillations

of the wheelset-track system probably occur on the low rails and inner wheels. Except for mode shape shown in Figure 10(h), in which the unstable oscillation occurs on inner wheels of leading and trailing wheelsets, other unstable oscillations mainly occur on the inner wheels of leading wheelsets. Particularly, the mode shape shown in Figure 10(g) presents that the deformations of low rail and inner wheels of leading wheelsets are obvious when the corresponding negative damping ratio is the smallest. The unstable oscillation is most likely to occur in the case, whose negative damping ratio is -0.03613 and the relevant unstable oscillation frequency is 473.80 Hz. Furthermore, the main unstable oscillations corresponding to the least negative damping ratios with curve radius from 200 m to 500 m all take place on the low rail and relevant inner wheel of leading wheelset. Therefore, it can be concluded that the friction-induced oscillations of the wheelset-track system on tight curved tracks primarily generates on the low rail, which means the rail corrugations on tight curved tracks mainly appears on the low rail.

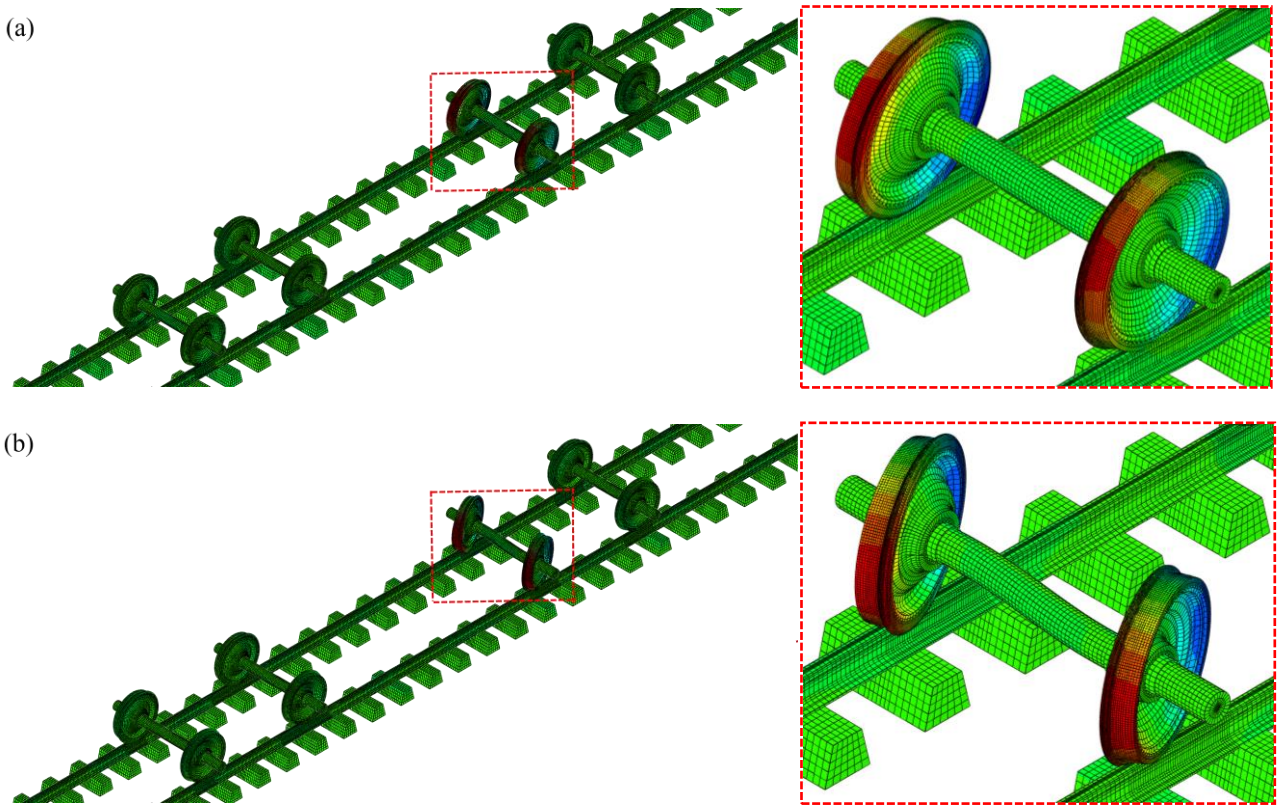

(c)

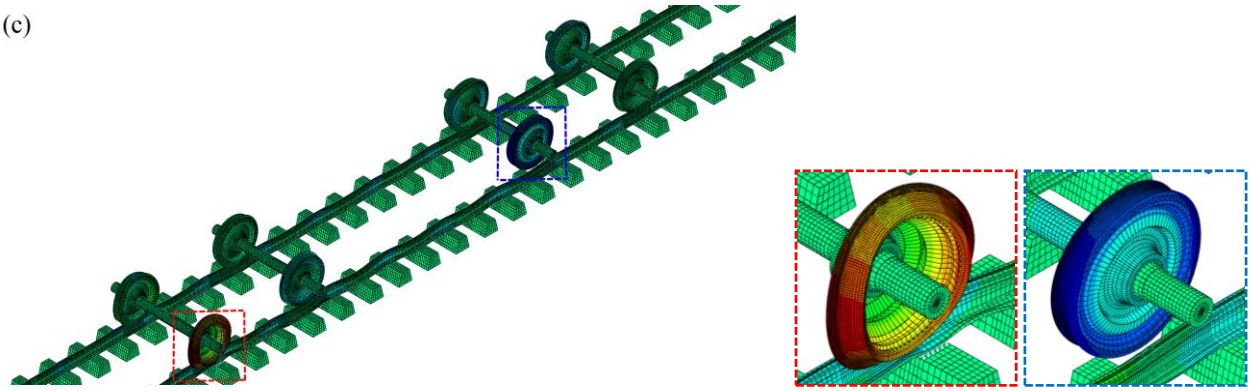

(d)

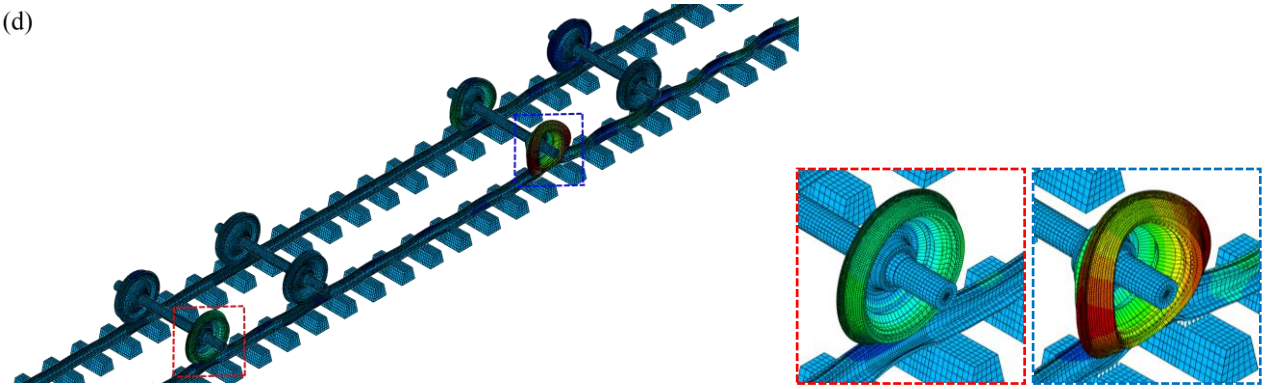

(e)

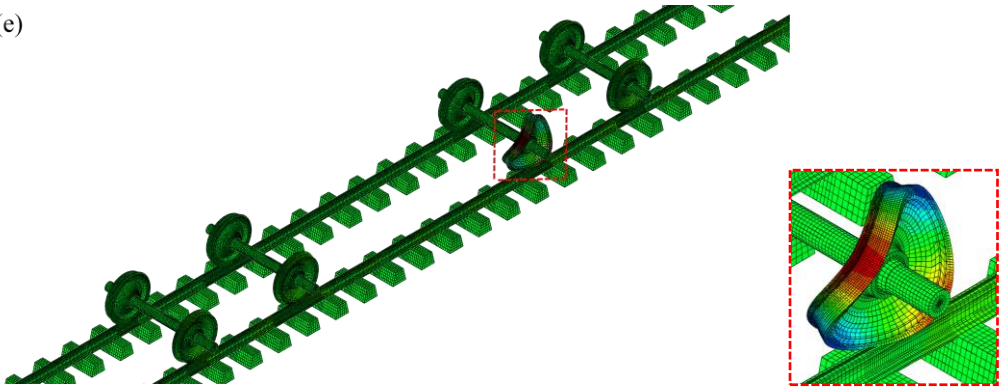

(f)

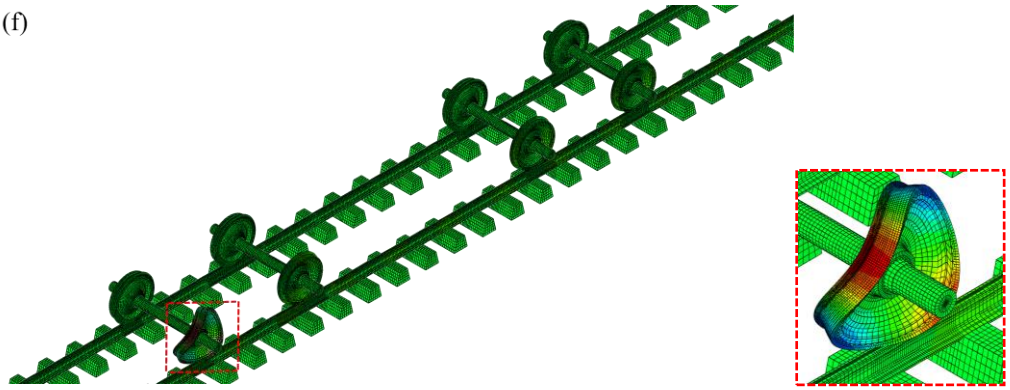

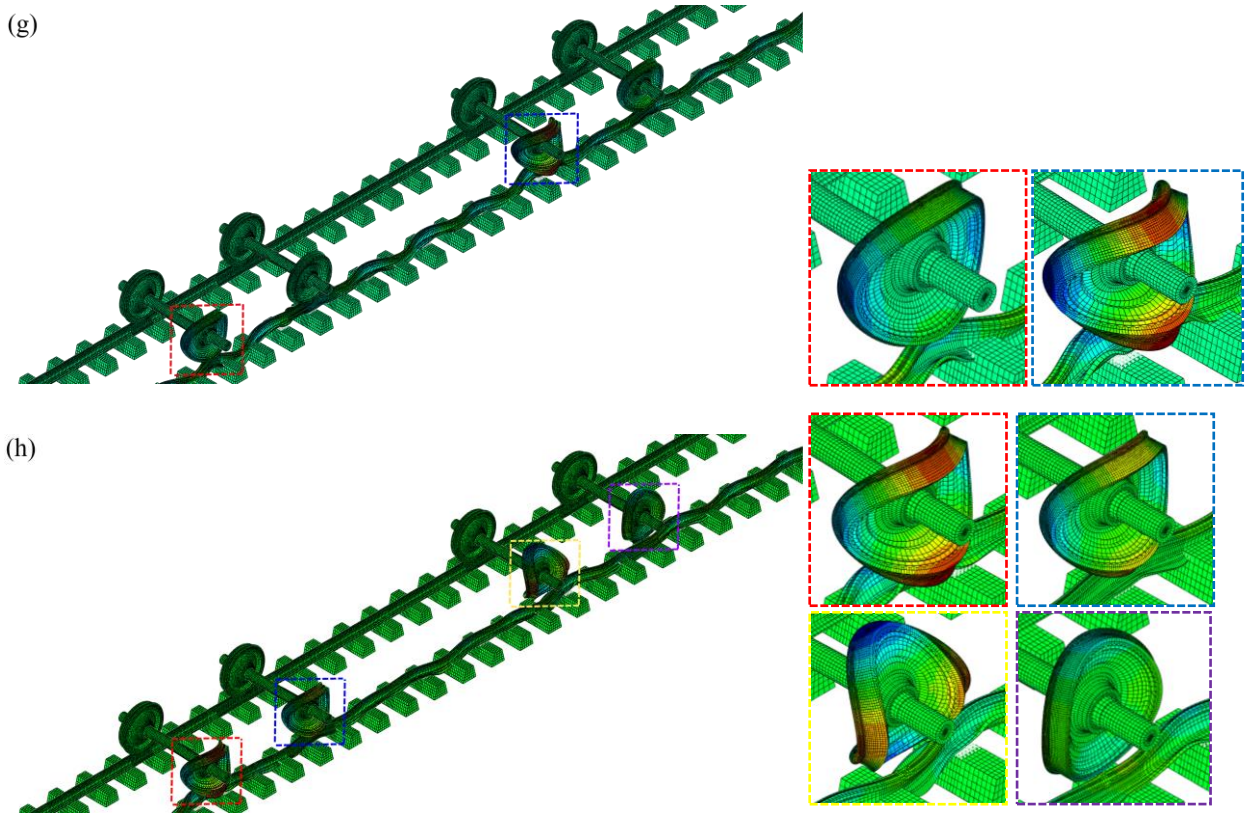

Figure 10. Mode shapes of the unstable vibrations of the wheelset-track system (R = 300 m): (a) ξ = -0.00022, f = 229.32 Hz; (b) ξ = -0.00012, f = 230.48 Hz; (c) ξ = -0.00422, f = 451.34 Hz; (d) ξ = -0.00178, f = 451.63 Hz; (e) ξ = -0.00025, f = 469.08 Hz; (f) ξ = -0.00011, f = 469.24 Hz; (g) ξ = -0.03613, f = 473.80 Hz; (h) ξ = -0.02763, f = 474.50 Hz

Discussion

The above simulations perform the creep force analyses and the friction-induced oscillation analyses of the wheelset-track systems in different curve radii. According to the creep force analyses, when the radius of a curved track is less than 450 m, the creep forces on both the outer and inner wheels of the leading wheelset of each bogie always tend to be saturated, while those on the outer and inner wheels of the trailing wheelset are still unsaturated in the curve radius range of 200-800 m. According to the friction-induced oscillation analyses, when the radius of a curved track is less than 500 m, the friction-induced oscillation is apt to occur, while the friction-induced oscillation rarely occurs when the curve radius changes from 550 m to 800 m. The relationship between the creep

force and the friction-induced oscillation is discussed as follows.

Firstly, the saturated creep forces on both wheels of leading wheelset cause the friction-induced oscillation of the wheelset-track system when the curved radius is less than 450 m. But the friction-induced oscillation also easily generates when the curve radius is 500 m. The difference of curve radius ranges is mainly because it is assumed that the creep force between the wheel and rail can be regarded as saturated when the deviation between the creep force and friction force is less than 5%. Then, there is a large difference between the occurrence probabilities of friction-induced oscillation on the low rail of a tight curved track and that on the high rail of the identical tight curved track. The dominant friction-induced oscillation mostly takes place on the low rail, while that hardly occurs on the high rail even the creep force on the outer wheel of the leading wheelset is saturated. In general, in the curved track of radius 200-550 m, the contact angle between the outer wheel and high rail is about 14.43-29.19^{o,} and the contact angle between the inner wheel and low rail is about 1.50-1.78^{o}. Therefore, the phenomena in tight curves can be explained according to Ref. [31], which predicted that when the contact angle is larger than 8.41^{o} even the creep force is saturated, the friction-induced oscillation of the wheelset-track system seldom occurs. Next, with the curve radius increases from 550 m to 800 m, the creep force on the outer wheel of the leading wheelset in this range is still saturated, but the friction-induced oscillation rarely occurs due to the change of the direction of the saturated creep force [31]. Besides, the creep force on the outer wheel of the leading wheelset is further studied with increasing the curve radius above 800 m. It can be found that when the curve radius is larger than 1000 m, the creep force on the outer wheel of the leading wheelset trends to be unsaturated. It means that the friction-induced oscillation is more difficult to occur with increasing the curve radius.

Conclusions

According to the field investigations in Chinese metros, there is a typical phenomenon of rail corrugation in metro lines, which is still difficult to be solved so far. It can be found that corrugation easily occurs on the low rails of the sharp curved tracks whose curve radii are less than 350 m, but rarely occurs on the high rails of the same tracks, and rail corrugations seldom occur on both low and high rails of the curved tracks whose curve radii are larger than 650-800 m. The purpose of the present paper is to explain the general phenomenon of rail corrugation from the perspective of the correlation between the friction-induced oscillation of wheelset-track system and curve radius. Therefore, the effects of the curve radius on the creep force between wheel and rail and the friction-induced oscillation of the wheelset-track system are investigated, respectively. It can be summarized that there is a proportional relation between the creep force and friction-induced oscillation. Comparing the numerical simulation results with the field investigations on metros in China, the following conclusions can be drawn.

(1) When the radius of a curved track is less than 450 m, the creep forces on both the outer and inner wheels of the leading wheelset of each bogie always trend to be saturated, while those on the outer and inner wheels of the trailing wheelset are still unsaturated for a curve radius range of 200-800 m. Besides, when the radius of a curved track is less than 500 m, the friction-induced oscillation is apt to occur, but it rarely occurs when the curve radius is above 500 m. The occurrence possibility of rail corrugation decreases with increasing curve radius from 200 m to 500 m.

(2) When the radius of a curved track is less than 350 m, the saturated creep force easily induces friction-induced oscillation of the inner wheel-low rail system, but it cannot induce friction-induced

oscillation of the outer wheel-high rail system due to a large contact angle between the outer wheel and high rail. Therefore, the reason why there is such a large difference between the occurrence probability of rail corrugation on the low rail of a tight curved track and that on the high rail of the identical tight curved track is attributed to the difference in the contact angle.

(3) When the radius of a curved track is larger than 650-800 m, although only the creep force on the outer wheel of the leading wheelset is saturated, no friction-induced oscillation of the wheelset-track system occurs due to the direction of the saturated creep force. With the curve radius increases sequentially, the creep forces on both the outer and inner wheels of the leading wheelset trend to be unsaturated.

Acknowledgement

The authors thank the financial support from the National Natural Science Foundation of China (Grant No: 51805057), the Basic Natural Science and Frontier Technology Research Program of the Chongqing Municipal Science and Technology Commission (Grant No: cstc2018jcyjA2567) and the Chongqing Municipal Key Laboratory Open Fund for Integration and Control of Urban Rail Transit Vehicle Systems (Grant No: CKLURTSIC-KFKT-201802).

References

[1] Grassie SL. Rail corrugation: advances in measurement, understanding and treatment. *Wear*. 2005; 258: 1224-34.

[2] Sato Y, Matsumoto A, Knothe K. Review on rail corrugation studies. *Urban Rapid Rail Transit*. 2010; 253: 130-9.

[3] Correa N, Vadillo E, Santamaria J, et al. A versatile method in the space domain to study short-wave rail undulatory

wear caused by rail surface defects. *Wear*. 2016; 352: 196-208.

[4] Li W, Wang H, Wen Z, et al. An investigation into the mechanism of metro rail corrugation using experimental and theoretical methods. *Proc IMechE Part F: Journal of Rail and Rapid Transport.* 2016; 230: 1025-39.

[5] Wei K, Liang D, Mei M, et al. Preforming behaviors of carbon fiber fabrics with different contents of binder and under various process parameters. *Composites Part B: Engineering*. 2019, 166: 211-32.

[6] Zhang H, Liu W, Liu W, et al. Study on the cause and treatment of rail corrugation for Beijing metro. *Wear*. 2014; 317: 120-8.

[7] Vila P, Baeza L, Martínez-Casas J, et al. Rail corrugation growth accounting for the flexibility and rotation of the wheel set and the non-Hertzian and non-steady-state effects at contact patch. *Vehicle Syst Dyn*. 2014; 52: 92-108.

[8] Andersson R, Torstensson PT, Kabo E, et al. The influence of rail surface irregularities on contact forces and local stresses. *Vehicle Syst Dyn*. 2015; 53: 68-87.

[9] Wu TX, Thompson DJ. An investigation into rail corrugation due to micro-slip under multiple wheel/rail interactions. *Wear.* 2005; 258: 1115-25.

[10] Sun YQ, Simson S. Wagon-track modelling and parametric study on rail corrugation initiation due to wheel stick-slip process on curved track. *Wear*. 2008; 265: 1193-201.

[11] Saulot A, Descartes S, Berthier Y. Sharp curved track corrugation: From corrugation observed on-site, to corrugation reproduced on simulators. *Tribol Int*. 2009; 42: 1691-705.

[12] Ren L, Xie G, Iwnicki SD. Properties of wheel/rail longitudinal creep force due to sinusoidal short pitch corrugation on railway rails. *Wear*. 2012; 284-285: 73-81.

[13] Egana JI, Vinolas J, Gil-Negrete N. Effect of liquid high positive friction (HPF) modifier on wheel-rail contact and rail corrugation. *Tribol Int*. 2005; 38: 769-74.

[14] Chen GX, Zhou ZR, Ouyang H, et al. A finite element study on rail corrugation based on saturated creep force-induced self-excited vibration of a wheelset-track system. *J Sound Vib*. 2010; 329: 4643-55.

[15] Kurzeck B. Combined friction induced oscillations of wheelset and track during the curving of metros and their influence on corrugation. *Wear*. 2011; 271: 299-310.

[16] Wen Z, Jin X, Xiao X, et al. Effect of a scratch on curved rail on initiation and evolution of plastic deformation induced rail corrugation. *Int J Solids Struct*. 2008; 45: 2077-96.

[17] Saulot A, Descartes S, Berthier Y. Sharp curved track corrugation: From corrugation observed on-site, to corrugation reproduced on simulators. *Tribol Int*. 2009; 42: 1691-705.

[18] Torstensson PT, Schilke M. Rail corrugation growth on small radius curves - Measurements and validation of a numerical prediction model. *Wear*. 2013; 303: 381-96.

[19] Eadie DT, Santoro M, Oldknow K, et al. Field studies of the effect of friction modifiers on short pitch corrugation generation in curves. *Wear*. 2008; 265: 1212-21.

[20] Meehan PA, Batten RD, Bellette PA. The effect of non-uniform train speed distribution on rail corrugation growth in curves/corners. *Wear*. 2016; 366-367: 27-37

[21] Cui XL, Chen GX, Zhao JW, et al. Field investigation and numerical study of the rail corrugation caused by frictional self-excited vibration. *Wear*. 2017; 376: 1919-29.

[22] Qian WJ, Chen GX, Ouyang H, et al. A transient dynamic study of the self-excited vibration of a railway wheel set-track system induced by saturated creep forces. *Vehicle Syst Dyn*. 2014; 52: 1115-38.

[23] Hu WP, Wang P, Chen GX, et al. Experimental Study on Corrugation of a Sliding Surface Caused by Frictional Self-Excited Vibration. *Tribol T.* 2016; 59: 8-16.

[24] Archard JF. Contact and Rubbing of Flat Surfaces. *J Appl Phys*. 1953; 24: 981-8.

[25] Brockley CA, Ko PL. An investigation of rail corrugation using friction-induced vibration theory. *Wear*. 1988; 128: 99-105.

[26] Chen GS. Handbook of Friction-Vibration Interactions. *Elsevier Press*. 2014.

[27] Qian WJ, Huang Z, Ouyang H, et al. Numerical investigation of the effects of rail vibration absorbers on wear behaviour of rail surface. *Proc IMechE Part J: Journal of Engineering Tribology*, 2018; 0(0), 1350650118785061.

[28] Pilipchuk VN, Ibrahim RA, Blaschke PG. Disc Brake Ring-Element Modeling Involving Friction-Induced Vibration. *J Vib Control*. 2002; 8(8): 1085-104.

[29] Abd RA, Ouyang H. Complex eigenvalue analysis and dynamic transient in predicting disc brake squeal. *Vehicle Syst Dyn*. 2006; 2: 143-55.

[30] Adams GG. Self-excited oscillations of two elastic half-spaces sliding with a constant coefficient of friction. *J Appl Mech*. 1995; 62(4): 867.

[31] Cui XL, Chen GX, Yang HG, et al. Effect of the wheel/rail contact angle and the direction of the saturated creep force on rail corrugation. *Wear*. 2015; 330: 554-62.